Nano Energy 77 (2020) 105152

Contents lists available at ScienceDirect

Nano Energy

journal homepage: http://www.elsevier.com/locate/nanoen

# Enhanced photocurrent via ferro-pyro-phototronic effect in ferroelectric $BaTiO_3$ materials for a self-powered flexible photodetector system

Kun Zhao [a,b], Bangsen Ouyang [a,d], Chris R. Bowen [c], Ya Yang [a,d,e,*]

[a] CAS Center for Excellence in Nanoscience, Beijing Key Laboratory of Micro-nano Energy and Sensor, Beijing Institute of Nanoenergy and Nanosystems, Chinese Academy of Sciences, Beijing, 100083, PR China
[b] State Key Laboratory of Advanced Processing and Recycling of Nonferrous Metals, Lanzhou University of Technology, Lanzhou, 730050, PR China
[c] Department of Mechanical Engineering, University of Bath, BA2 7AK, UK
[d] School of Nanoscience and Technology, University of Chinese Academy of Sciences, Beijing, 100049, PR China
[e] Center on Nanoenergy Research, School of Physical Science and Technology, Guangxi University, Nanning, 530004, PR China

ARTICLE INFO

*Keywords:*
$BaTiO_3$
Ferro-pyro-phototronic effect
Photodetector systems
Photovoltaic effect
Pyroelectric effect

ABSTRACT

Some ferroelectric materials have demonstrated both pyroelectric and photovoltaic effects for scavenging thermal and solar energies. However, how to couple pyroelectric and photovoltaic effects in ferroelectric materials remains a challenge. Here, a ferro-pyro-phototronic effect based on coupling pyroelectric and photovoltaic effects has been utilized to enhance the photocurrent in a ferroelectric $BaTiO_3$-based flexible photodetector system. As compared with a purely photovoltaic system, the corresponding current peak and plateau were 451.9% and 17.2% higher in the coupled photovoltaic-pyroelectric system, respectively. The results can be explained by ferro-pyro-phototronic effect with an induced energy band bending. As a demonstration of its potential application, we developed a sensing system that is suitable for detecting and recognizing both light and temperature variations by recording the electrical signals mapped as an array.

## 1. Introduction

With the urgent requirement for low in cost, clean and renewable new energy, it is critical to develop low power micro/nano sensors and self-powered nano-devices [1–6]. For this reason, a variety of novel micro/nano devices have been designed by using some physical effects including photovoltaic [7–9], pyroelectric effect [10–12], thermoelectricity [13–15] and piezoelectricity [16–18] in order to directly convert light, thermal and mechanical energies into electricity. Significantly, ferroelectric materials such as $BiFeO_3$ (BFO) [19–21], $Pb(Zr,Ti)O_3$ (PZT) [22,23], $BaTiO_3$ (BTO) [24–26], and $LiNbO_3$ [27–29] have made important progress in heat, light, and pressure conversion in recent years. However, the majority of such devices are only able to convert a single source of energy into electrical energy, thus lead to more expensive and lower power conversion efficiencies, which has influenced and limited their widespread application in fields such as public security, wearables, robotics and internet of things. Thus, it is necessary to develop multifunctional devices that are able to harvest multiple sources of energy simultaneously. Our group has investigated BTO material devices with illumination owing to a photovoltaic-pyroelectric coupled effect [30] and combined pyro-piezoelectric effect [31] for detecting and measuring temperature/pressure signals. However, there has been no report about the enhancement of the photocurrent in ferroelectric BTO materials via a ferro-pyro-phototronic effect by coupling photovoltaic and pyroelectric effects as for self-powered flexible photodetector systems. Such devices are of interest to detect light and environmental temperature changes in order to achieve simultaneous multi-signal sensing and exploit electrical energy from light-temperature coupling.

Here, we present a simple, reliable and effective method to modulate energy band structure of BTO. An increase of photocurrent was obtained using a ferro-pyro-phototronic effect. Moreover, a photodetector system was designed for sensoring both light and temperature variation not using battery or supercapacitor. A BTO ceramic sheet was used with the light-facing side overlapping indium tin oxide (ITO) electrode and the non-illuminated side having a Ag electrode. A soft kapton membrane allows the device to be both flexible and easily integrated into a sensor array, thereby providing potential applications in the field of wearable

* Corresponding author. CAS Center for Excellence in Nanoscience, Beijing Key Laboratory of Micro-nano Energy and Sensor, Beijing Institute of Nanoenergy and Nanosystems, Chinese Academy of Sciences, Beijing, 100083, PR China.
*E-mail address:* yayang@binn.cas.cn (Y. Yang).

https://doi.org/10.1016/j.nanoen.2020.105152
Received 26 May 2020; Received in revised form 19 June 2020; Accepted 28 June 2020
Available online 26 July 2020
2211-2855/

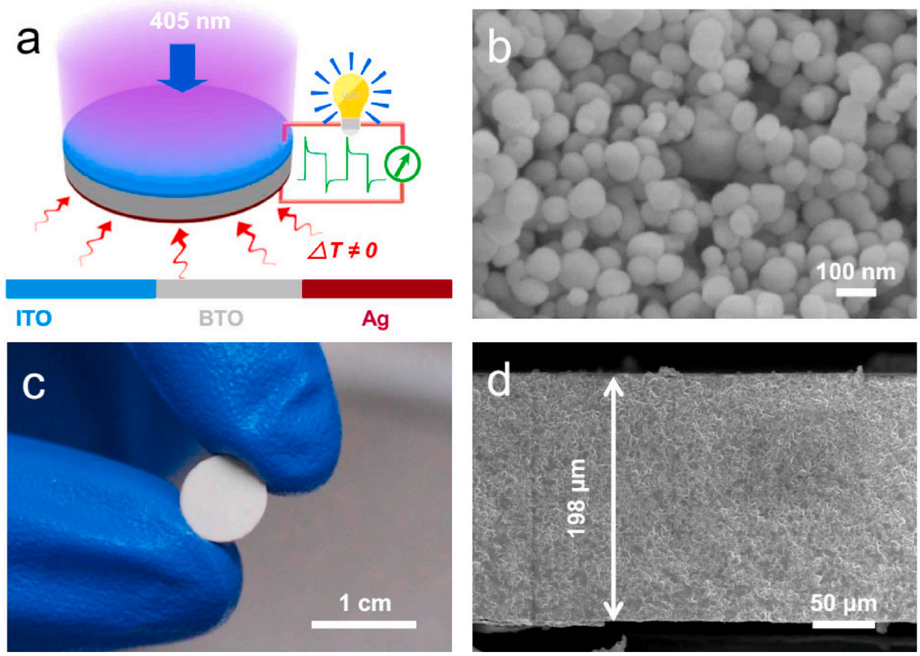


**Fig. 1.** Structural characterization of the ITO/BTO/Ag device. (**a**) A schematic illustration of the fabricated device structure based on BTO. (**b**) The morphology of the BTO particles was examined using SEM. (**c**) Photograph of a single device. (**d**) Thickness of the fabricated device observed by SEM.

electronics, environmental sensors and artificial intelligent sensors. The system cannot only be used to detect individual sources of light and temperature change accurately, but is able to respond to both light and temperature variation when applied simultaneously. Mapping image of voltages for 4 × 4 array can be obtained synchronously in real time. Under "light + heating" (7.78 mW/cm$^2$, $\triangle T = 22.1$ K) condition, the photodetector was able to generate a coupled current peak that was 451.9% higher than by illumination alone due to the ferro-pyro-phototronic effect. In addition, when under "light + cooling" (7.78 mW/cm$^2$, $\triangle T = -14.5$ K) condition, the photodetector can generate a stable current plateau that is enhanced by 17.2%. Moreover, the voltages of photodetector system were synchronously obtained in real time to create a mapping image from light and temperature changes. The single source or coupled information can be ascertained by analyzing the output current/voltage and this novel form of self-powered flexible photodetector system provides a new approach for rapid and accurate detection of light-temperature coupled signals. More importantly, as compared with the reported investigations [24,26,30,38], this work presents a self-powered flexible photodetector system based on photovoltaic and pyroelectric effects by using a ferroelectric BTO ceramic sheet as the sensor unit for detecting the 405 nm light intensity and temperature without using external power source. Moreover, there is no interference among each units of the fabricated flexible self-powered system, which makes the foundation for preparing more arrays of self-powered flexible photodetector system.

## 2. Experimental section

### 2.1. Preparation of BTO ceramic sheets

Firstly, a few drops of polyvinyl alcohol (PVA)-water solution (2 wt %) were completely mixed with 0.3 g BTO nanoparticles. Secondly, the fine powder was poured into a mould with a diameter of 10 mm, and it was compacted into wafers by a uniaxial pressure of 2.5 MPa with a powder compression machine. Finally, after eliminate the PVA at 650 °C for 1 h, the BTO sheets were sintered at 1200 °C for 2 h.

### 2.2. Fabrication of the devices

Initially, the two sides of the BTO ceramic sheets were covered with Ag electrode by DC magnetron sputtering system (Beijing jinshengweina technology Co. MSP-820). Then, the devices were polarized by an electric field of 2.3 kV/mm for 30 min. Moreover, one Ag electrode was removed and polished the device to a thickness of ~200 μm. Lastly, ITO films was coated with the polished surface via RF magnetron sputtering under power of 150 W for 15 min. The 4 × 4 matrix flexible photodetector system was constructed by a 16 ITO/BTO/Ag devices and a piece of 50 mm × 50 mm × 0.03 mm kapton membrane.

### 2.3. Characterization and measurements

The crystal structures were analyzed by an X-ray diffractometer (Panalytical X'pert powder, Cu Kα radiation). The morphologies of materials were obtained by a scanning electron microscope (Hitachi SU8020). The piezoelectric coefficient $d_{33}$ has been measured by a Quasi-static $d_{33}$ measuring instrument (Institute of Acoustics, Chinese Academy of Sciences, ZJ-4AN). The temperature data and images were measured by an infrared thermographic camera (Optris PI400). The output current signals were performed using a current preamplifier (Stanford Research SR570). The voltage signals were tested by a preamplifier (Stanford Research SR560). The corresponding output voltage signals and mapping image of the self-powered flexible system were recorded on a multichannel data acquisition system (National Instruments NI PXle-1082).

## 3. Results and discussion

A schematic diagram of the designed device subjected to simultaneous illumination and a temperature variation is illustrated in Fig. 1a, which consists of an upper transparent ITO electrode, a BTO ceramic sheet and a lower Ag electrode. Fig. 1b presents BTO particles of less than 50–100 nm in diameter prior to sintering, and the corresponding scanning electron microscopy (SEM) image at low magnification is shown in Fig. S1a (Supporting Information). After sintering at 1200 °C, the X-ray diffraction patterns (Fig. S1b, Supporting Information) show

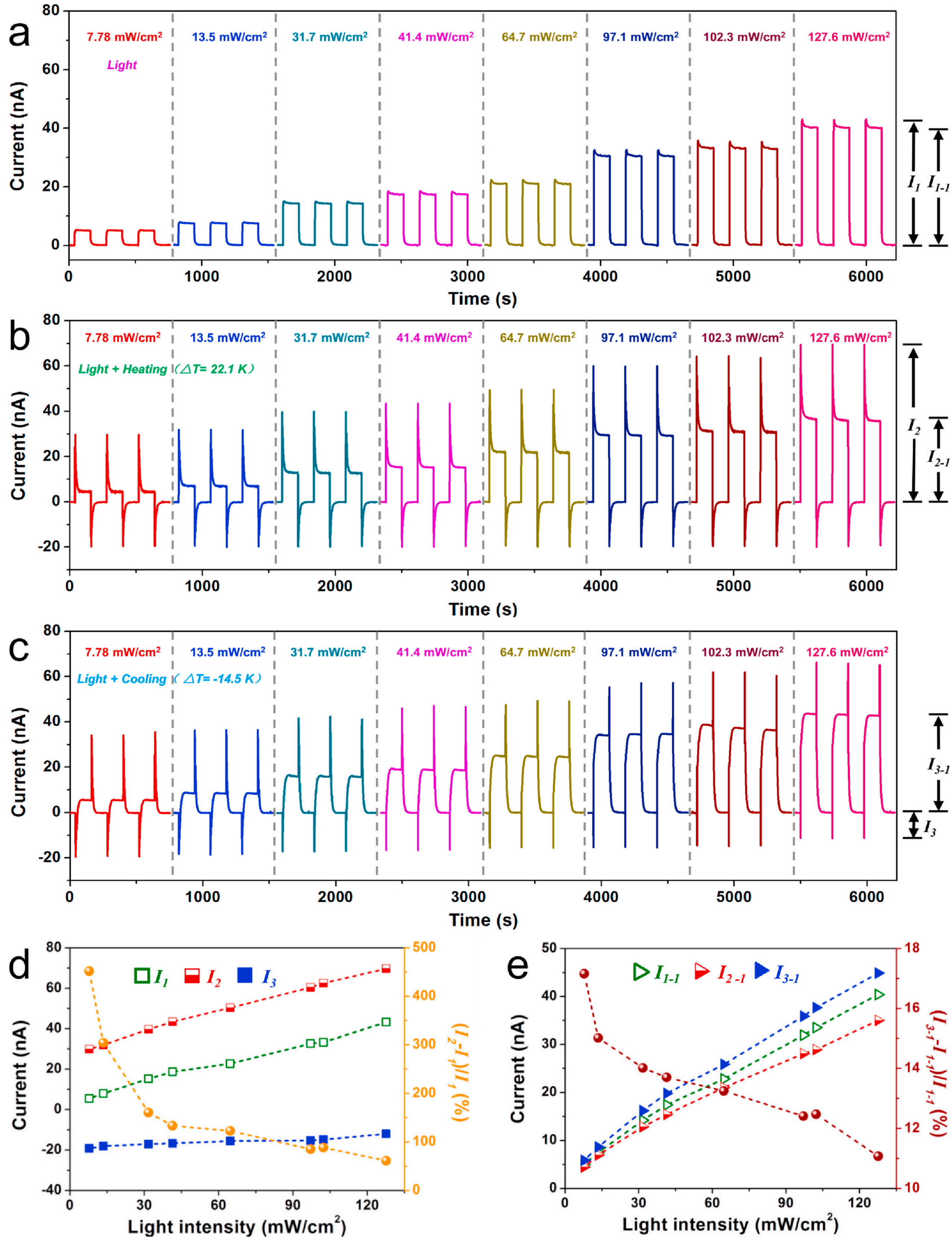


**Fig. 2.** Detector performance. (**a**) Measured currents of the detector under different light intensities. (**b,c**) Measured currents of the detector with "light + heating" (b) and "light + cooling" (c) states. (**d**) The current peak and current peak enhanced ratios under different conditions; where the $I_1$, $I_2$ and $I_3$ are current peak under "light", "light + heating" and "light + cooling" states. The current peak ratios under "light + heating" state can be calculated by the equation of $[(I_2–I_1)/I_1] \times 100\%$. (**e**) The current plateau and plateau enhanced ratios under different conditions; where the $I_{1\text{-}1}$, $I_{2\text{-}1}$ and $I_{3\text{-}1}$ are current plateau under "light", "light + heating" and "light + cooling" states. The current plateau ratios under "light + cooling" state can be calculated by the equation of $[(I_{3\text{-}1}- I_{1\text{-}1})/I_{1\text{-}1}] \times 100\%$.

that the peak of BTO particles at $2\theta = 45.2^\circ$ is divided into two peaks at $2\theta = 44.9^\circ$ and $2\theta = 45.5^\circ$. This indicates that the BTO ceramic sheets have an orthorhombic phase, which provides the materials with a spontaneous polarization. The surface and cross-sectional SEM images of BTO ceramic sheets shows that the average grain size was about 140–400 nm and the structure was compact and dense, see Figs. S1c–S1f (Supporting Information). Fig. 1c and d shows a photograph and SEM image of the fabricated devices which acts as the base unit for the self-powered flexible photodetector system, the diameter and thickness of BTO ceramic sheet are approximately 8 mm and ~200 μm, respectively. The piezoelectric coefficient $d_{33}$ of the polarized ITO/BTO/Ag was about 310 pC/N.

Fig. 2a presents the currents of the detector under different illumination intensities at room temperature, where the current peaks ($I_1$) and current plateaus ($I_{1\text{-}1}$) signals can be increased from 5.4 nA to 43.2 nA and from 5 nA to 40 nA with increasing the illumination intensity from 7.78 mW/cm$^2$ to 127.6 mW/cm$^2$, respectively. As illustrated in Fig. 2b, the measured current of detector appear trend of a distinct sharp peak followed by a lower steady plateau when illumination and being subjected to a constant higher temperature ($\triangle T = 22.1$ K) simultaneously. The current peaks ($I_2$) and current plateaus ($I_{2\text{-}1}$) of the device can be increased from 29.8 nA to 69.7 nA and from 4.46 nA to 35 nA by increasing the illumination intensity from 7.78 mW/cm$^2$ to 127.6 mW/cm$^2$ and a temperature variation ($\triangle T = 22.1$ K), respectively. On comparing the data in Fig. 2a and b, it shows that the current peaks owing to ferro-pyro-phototronic effect increase with increasing light intensity and are larger than when illumination alone. However, the coupled current plateau is smaller compared to illumination alone. In addition, the currents of ITO/BTO/Ag detector with light intensities ranging from 7.78 mW/cm$^2$ to 127.6 mW/cm$^2$ and a constant lower temperature of $\triangle T = -14.5$ K simultaneously are illustrated in Fig. 2c. It is observed that the current peak signals ($I_3$) due to the ferro-pyro-phototronic effect decreases from −19.2 nA to −12 nA but the current plateau signals ($I_{3\text{-}1}$) are increased from 5.9 nA to 44.9 nA with increasing the illumination intensity from 7.78 mW/cm$^2$ to 127.6 mW/cm$^2$ at $\triangle T = -14.5$ K. The current plateau signals were show to be dramatically increased by use of a cooling temperature.

To confirm that the electrical signals of the device are a result of photovoltaic or pyroelectric effects, the voltages and currents were tested under illumination, heating and cooling states, see Fig. S2 (Supporting Information). In a normal forward connection, an upward voltage/current signal was obtained under illumination state (127.6 mW/cm$^2$) (Figs. S2a and S2b, Supporting Information). At a reversed connection, opposing polarity voltage/current signals were observed under the same light intensity (Figs. S2c and S2d, Supporting Information). In addition, the voltage/current signals of the device were observed to periodically change under conditions of cooling ($\triangle T = -14.5$ K) (Figs. S2e and S2f, Supporting Information) and heating ($\triangle T = 22.1$ K), as seen in Figs. S2g and S2h, Supporting Information).

Fig. 2d and e shows the change of photocurrent peak signals/signal enhancement ratio and photocurrent plateau signals/signal enhancement ratio under different conditions, respectively. The current signal enhancement ratios of the detector under both "light + heating" and "light + cooling" states can be calculated by the equations of $[(I_2 - I_1)/I_1] \times 100\%$ and $[(I_{3\text{-}1}\text{-}I_{1\text{-}1})/I_{1\text{-}1}] \times 100\%$, respectively; where the $I_1$, $I_2$ and $I_3$ are current peak with "light", "light + heating" and "light + cooling" conditions. The results show that heating would be used to boost the photocurrent peak and cooling would be used to increase the photocurrent plateau of the fabricated detector.

Under an illumination condition of 7.78 mW/cm$^2$, the output current peaks of the device at the "light + heating" and "light" are 29.8 nA and 5.4 nA, respectively. According to the equation of $[(I_2 - I_1)/I_1] \times 100\%$, the device at the "light + heating" ($\triangle T = 22.1$ K) state generated a coupled photocurrent peak that was 451.9% higher than light alone due to ferro-pyro-phototronic effect, the "light + heating" coupled photocurrent peak enhancement ratio was 61.3% higher than under light alone at an intensity of 127.6 mW/cm$^2$; see Fig. 2d. Under the condition of "light + heating", the current signals of the light and heating states are in the same direction, and the initial current can be considered as a superposition. The increase in the current peak is bound up with the temperature difference of the detector surface, while the decrease in output coupled photocurrent plateau may be the result of a decrease in the BTO layer polarization charge caused by due to the thermal vibrations.

Interestingly, the photocurrent plateau can be enhanced about 17.2% by "light + cooling " ($\triangle T = -14.5$ K) compared with the device under light alone at 7.78 mW/cm$^2$, which can be calculated by the equation of $[(I_{3\text{-}1} - I_{1\text{-}1})/I_{1\text{-}1}] \times 100\%$, the output current plateaus of device at the "light + cooling" and "light" are 5.86 nA and 5 nA, respectively. The "light + cooling" coupled photocurrent plateau enhancement ratio was 11.1% higher than under light alone at 127.6 mW/cm$^2$ (Fig. 2e). It is worth noting that there is a decrease in the enhancement ratios of the output photocurrent signals with increasing light intensity. Under the condition of "light + cooling", there is a decrease in current peak of the device since the initial current signals of the light and cooling states are in opposing directions, while the increased of the output coupled photocurrent plateau may be the result of the increase in BTO layer polarization due to lower thermal vibrations.

The corresponding voltages and enhancement ratios with "light", "light + heating" and "light + cooling" states were found to follow a similar trend with current information, as seen in Fig. S8 (Supporting Information). Where the voltage enhancement ratios are calculated with "light + heating" and "light + cooling" states by the equations $[(V_2 – V_1)/V_1] \times 100\%$ and $[(V_{3\text{-}1}\text{-}V_{1\text{-}1})/V_{1\text{-}1}] \times 100\%$, respectively. The detector with light (7.78 mW/cm$^2$) and heating ($\triangle T = 22.1$ K) or cooling ($\triangle T = -14.5$ K) temperature simultaneously can generate a coupled photovoltage peak/plateau that was 391.5%/125% higher than light alone due to a coupled photovoltaic-pyroelectric effect. Moreover, under an illumination condition of 127.6 mW/cm$^2$, the detector at the "light + heating ($\triangle T = 22.1$ K)"/"light + cooling ($\triangle T = -14.5$ K) "state can generate a coupled photovoltage peak/plateau that was 50.9%/92.8% higher than light alone owing to ferro-pyro-phototronic effect.

For pyroelectric voltage/current, the working mechanism of the fabricated device can be related to the thermally induced random oscillation state of the dielectric dipoles around its equilibrium axis under room temperature [32], so that there is no output electric signal (Fig. S3a, Supporting Information). On heating, the temperature of the device increases and the original oscillation state of the dielectric dipoles is interferenced, it is to bring about the dielectric diploes oscillate to a larger degree. Meanwhile, the spontaneous polarization of ferroelectric BTO ceramics is weakened and the induced charges at the electrode are decreased, leading to a transfer of electrons from the left electrode (ITO) to the right electrode (Ag) (Fig. S3b, Supporting Information). Thus, a positive pyroelectric voltage/current is observed (Figs. S2e and S2f, Supporting Information).

During cooling, the dielectric dipoles oscillate to a smaller degree and the corresponding spontaneous polarization of ferroelectric BTO ceramics is strengthened, leading to a transfer of electrons from the right electrode (Ag) to the left electrode (ITO) (Fig. S3c, Supporting Information). Therefore, a negative pyroelectric voltage/current is observed (Figs. S2g and S2h, Supporting Information). The pyroelectric voltages, pyroelectric currents, charge densities and pyroelectric coefficients of the polarized BTO device are presented in Figs. S4–S6 (Supporting Information). A semiconductor heater is used to control the periodic heating conditions from 3.0 K to 22.1 K in Fig. S4a (Supporting Information). The positive voltage/current peaks are gradually increased from 0.13 V to 0.79 V/3.8 nA to 25.1 nA which correspond to heating variations shown in Figs. S4b and S6a (Supporting Information), respectively. In addition, a semiconductor cooler is applied to adjust the periodic cooling conditions from −2.4 K to −14.5 K in Fig. S5a (Supporting Information). The negative voltage/current peaks are increased

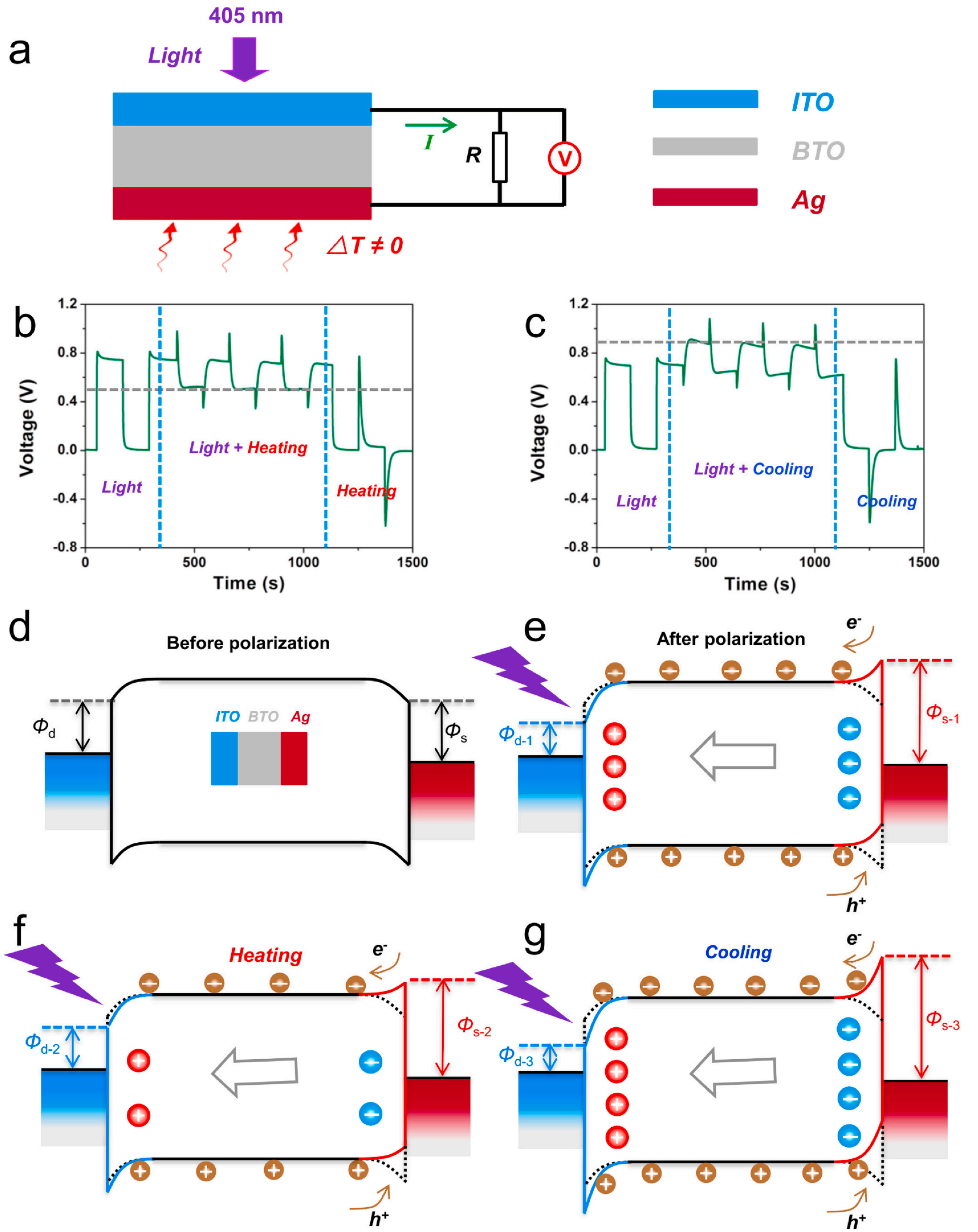


**Fig. 3.** Schematic diagram, measured voltage signals with ferro-pyro-phototronic effect and energy band diagrams of the detector. (**a**) Schematic of the voltage measurement of the detector. (**b**) Measured voltages of the photodetector under "light" (127.6 mW/cm$^2$), "light + heating" and "heating" ($\triangle T = 22.1$ K) states. (**c**) Measured voltages of the photodetector under "light" (127.6 mW/cm$^2$), "light + cooling" and "cooling" ($\triangle T = -14.5$ K) states. (**d-g**) Energy band diagrams for the detector: (d) Before polarization. (e) After polarization under "light" state. (f) After polarization under "light + heating" state. (g) After polarization under "light + cooling" state.

from −0.11 V to −0.67 V/−3.9 nA to −22.3 nA, which correspond to the cooling variations displayed in Figs. S5b and S6c (Supporting Information), respectively. Fig. S6b (Supporting Information) presents infrared images of the device surface at different heating (top) and cooling (bottom) temperatures, which can be recorded by using an infrared thermographic camera. The calculated charge densities and pyroelectric coefficients ($P_c$) of different temperature variations of the fabricated detector are illustrated in Figs. S6d and S6e. When the heating temperature increased from 3.0 K to 22.1 K, the charge density increased from 63.4 nC/cm$^2$ to 513.5 nC/cm$^2$, and the cooling temperature increased from −2.4 K to −14.5 K, the charge density increased from −68.4 nC/cm$^2$ to −577.3 nC/cm$^2$. Moreover, the pyroelectric coefficient can be expressed as following: $P_c = I/[A(dT/dt)]$, where $I$, $A$ and $dT/dt$ is the short circuit pyroelectric current, the electrode area of the device and the rate of change in temperature, respectively [33]. The corresponding pyroelectric coefficients of the device can be obtained to be approximately 13–19 nC/cm$^2$K (heating) and 22–42 nC/cm$^2$K (cooling), respectively. It is higher than our previous research (about 16 nC/cm$^2$K) under cooling condition [24].

To evaluate the sensitivity of the device to illumination, the photoconductive gain ($G$), responsivity ($R$) and specific detectivity ($D^*$) are three important parameters were obtained with different states from Figs. S7a and S7b (Supporting Information). The $G$ is described as the ratio between the number of charges from the electrodes per unit time and the number of photons from the ITO/BTO/Ag per unit time [34], as given by $G=(\triangle I_{ph}/e)/(PS/h\nu)$, here, $\triangle I_{ph}$ is the difference between the photocurrent with illumination and without illumination, $P$ is the incident power density, $S$ is the illumination area on the ITO/BTO/Ag, $e$ is the electronic charge, and $h\nu$ is the energy of photon. The $R$ reflects the response of the photocurrent to the illumination power [35], and can be confirmed by $R=\triangle I_{ph}/(PS)$. The $D^*$ describes the ability of measuring weak light source signals and exihibiting the noise in the environment, defined as $D^*=R/(2e \cdot I_d/S)^{1/2}$, of which $I_d$ is the current without illumination [36]. The values of $G_2$, $R_2$ and $D^*_2$ resulting from ferro-pyro-phototronic effect showed greater than $G_1$, $R_1$ and $D^*_1$ that derived from individual photovoltaic effect, which were initially enhanced rapidly and then became to be stable with the increase of illumination intensity. However, $G_1$, $R_1$ and $D^*_1$ exhibited a decrease with increasing light intensity. The main reason for this result is the large temperature difference in the experiment, which causes the initial currents generated by the coupling effect to be much larger than by the individual photovoltaic effect, but as the light intensity increases, the light response plays a leading role, and the value of $G$, $R$ and $D^*$ tends to be flat. Under light illumination of 7.78 mW/cm$^2$, the values of $G_2$, $R_2$ and $D^*_2$ were approximately 5.5 times larger than $G_1$, $R_1$ and $D^*_1$. Moreover, under light illumination of 126.7 mW/cm$^2$, the values of $G_2$, $R_2$ and $D^*_2$ were approximately 1.6 times larger than $G_1$, $R_1$ and $D^*_1$. Meanwhile, the recovery time and response time of the detector under illumination intensity of 127.6 mW/cm$^2$ were investigated (Figs. S7c and S7d, Supporting Information). They were obtained between 10% and 90% of the current under illumination when the illumination was turned on and off, respectively. The chart clearly shows that the response time and recovery time of the detector are approximately 0.88 s and 1.06 s, respectively. It indicates that the device has a fine photo-response property. The response time and recovery time of the device are slower than those of some semiconducting materials-based photodetectors, the possible reason may be related to the crystal boundary of BTO ceramic. And the greater the thickness of the device, the slower the separation of electron pairs and holes, resulting in a slow response time and recovery time.

Fig. 3a presents a schematic of the device voltage measurement with a 100 MΩ load resistance. To demonstrate the ferro-pyro-phototronic effect on the output electrical signals, the photovoltages of the device were measured under three different conditions, including "light" (127.6 mW/cm$^2$), "heating" ($\triangle T$ = 22.1 K) and "light + heating", as shown in Fig. 3b. The result observed that the photovoltage at conditions of "light + heating" state is not an easy addition of the photovoltages at "light" and "heating" states. Under the condition of "light + heating", the photovoltage plateau is decreased compared with "light", this attenuation may be related to a coupling of light and heating. Fig. 3c presents the coupling enhancement of the photovoltage plateau of the device can be explicitly see under the condition of "light + cooling", as it compared with "light" (127.6 mW/cm$^2$) and "cooling" alone ($\triangle T$ = −14.5 K) states.

The corresponding photocurrents and photovoltage/photocurrent signals under different illumination intensities from 127.6 mW/cm$^2$ to 7.78 mW/cm$^2$ on the detector show a similar change (Figs. S9–S12, Supporting Information). Fig. S13 (Supporting Information) presents a comparison of the measured output voltage plateau (Fig. S13a, Supporting Information) and current plateau (Fig. S13b, Supporting Information) under illumination by different intensities due to the photovoltaic-pyroelectric coupled effect (Figs. S9–S12, Supporting Information). We found that the photovoltage plateau can be increased from 0.16 V to 0.76 V when the illumination intensity increased from 7.78 mW/cm$^2$ to 127.6 mW/cm$^2$. The light-heating coupled photovoltage plateau can be increased from 0.14 V to 0.52 V and light-cooling coupled photovoltage plateau can be enhanced from 0.19 V to 0.92 V, respectively (Fig. S13a, Supporting Information). Under the same light intensity, the corresponding photocurrent plateaus of the detector shows a decreasing order between "light + cooling", "light "alone and "light + cooling" states.

The phenomenon for the enhancement of photocurrent plateau of the device would be explained by the ferro-pyro-phototronic effect on the energy band diagrams, as described in Fig. 3d–g. The structure of the fabricated ITO/BTO/Ag detector can be considered as a BTO layer trapped between $\Phi_d$ and $\Phi_s$ Schottky barriers at left and right interfaces, as in Fig. 3d. After polarized, a ferroelectric polarization is formed in the BTO sheet. The positive polarized charges are obtained in the left interface, which lead to the barrier height $\Phi_{d\text{-}1}$ is decreased. Meanwhile, the negative polarized charges are obtained in the right interface, which lead to the Schottky barrier height $\Phi_{s\text{-}1}$ is increased. As presented in Fig. 3e, the 405 nm illumination-induced electron pairs flow into the ITO electrode and holes flow into the Ag electrode, the output photocurrent signals are detected. Under light illumination state, when the device is subject to heating, the device temperature is increased, resulting in the polarization is decreased, the barrier height $\Phi_{d\text{-}2}$ get higher owing to the reduction of positive polarized charges in the BTO layer. Furthermore, the barrier height $\Phi_{s\text{-}2}$ becomes lower owing to the reduction of negative polarized charges of the BTO layer. as displayed in Fig. 3f. The barrier height $\Phi_{s\text{-}2}$ decrease acts to reduce the separation of hole-electron pairs, the barrier height $\Phi_{d\text{-}2}$ increase is unfavorable to the electrons flow, resulting in output a small photocurrent. However, under "light + cooling" state, the device temperature is decreased and the polarization is increased, the barrier height $\Phi_{s\text{-}3}$ can be strengthen owing to the polarized charges of the BTO layer are increased, which is a very important advantage for separate the illumination-induced hole and electron pairs. Meanwhile, a decrease of the barrier height $\Phi_{d\text{-}3}$ acts to accelerate the electrons flow. Therefore, the output photocurrent plateau of the device can be significantly increased under "light + cooling" condition, as depicted in Fig. 3g. Moreover, polarized charges have been shown to change energy band structure of ferroelectric materials [19,37]. In addition, the currents and voltages of the fabricated device under different loading resistances during light illumination and heating states were measured, as presented in Fig. S14 (Supporting Information). The measured curves show that the voltage of the detector increased from 8 mV to 1.58 V and current decreased from 40.2 nA to 1.75 nA at a light intensity of 127.6 mW/cm$^2$ with the increase of loading resistances ranged from 0.2 MΩ to 900 MΩ, respectively (Fig. S14a, Supporting Information). Under the heating only ($\triangle T$ = 22.1 K) condition, the output voltage of the device increased from 0.34 V to 4.7 V and current decreased from 22.9 nA to 4.9 nA with the increase of loading resistances from 15 MΩ to 960 MΩ, respectively (Fig. S14b,

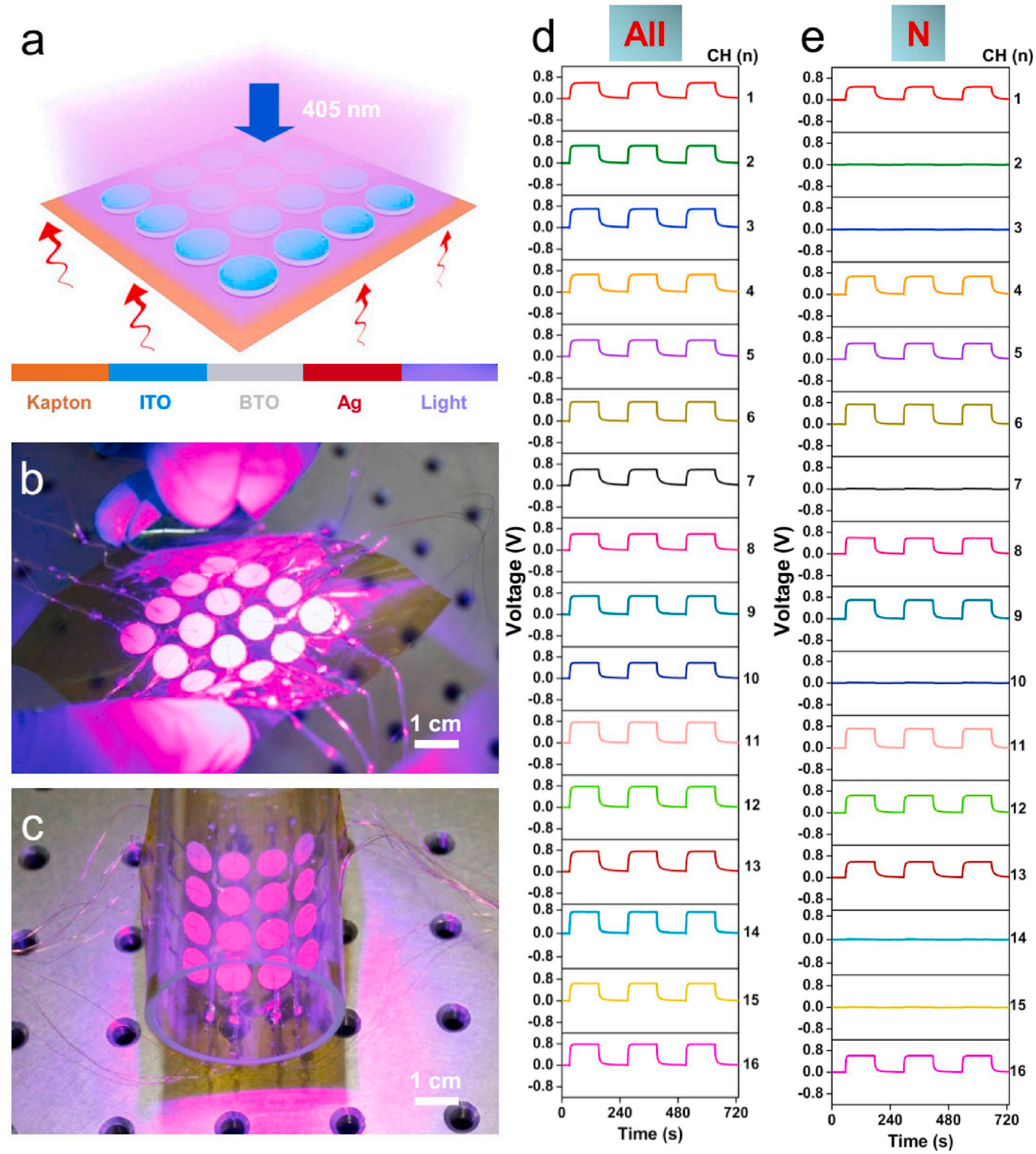


**Fig. 4.** A self-powered flexible photodetector system and *V-t* curves under 405 nm illumination. (**a**) Schematic of the designed flexible photodetector system. (**b**) Optical image showing the self-powered flexible photodetector system with 405 nm illumination in the bent state. (**c**) Optical image of the self-powered flexible photodetector system attached on a cylindrical acrylic pipe under 405 nm illumination to demonstrate flexibility. (**d,e**) *V-t* curves of the self-powered photodetector system under 405 nm illumination (127.6 mW/cm$^2$) through all channel (d) and a letter of "N" (e).

Supporting Information). It can be shown that the output voltage values increased with an increase of the loading resistance, while the current follows an opposite trend. According to the output electrical signals of the device at the "light ", "light + heating" and "light + cooling" states, it is obvious that the temperature has a great influence on the photocurrent, and the greater the cooling temperature, the larger the photocurrent [38]. Moreover, since the device has a metal/-ferroelectric/semiconductor structure of the device, it has rectifying characteristics [39]. Besides, the ferroelectric hysteresis loop of the ferroelectric material is critical to the material properties. [39–42], In

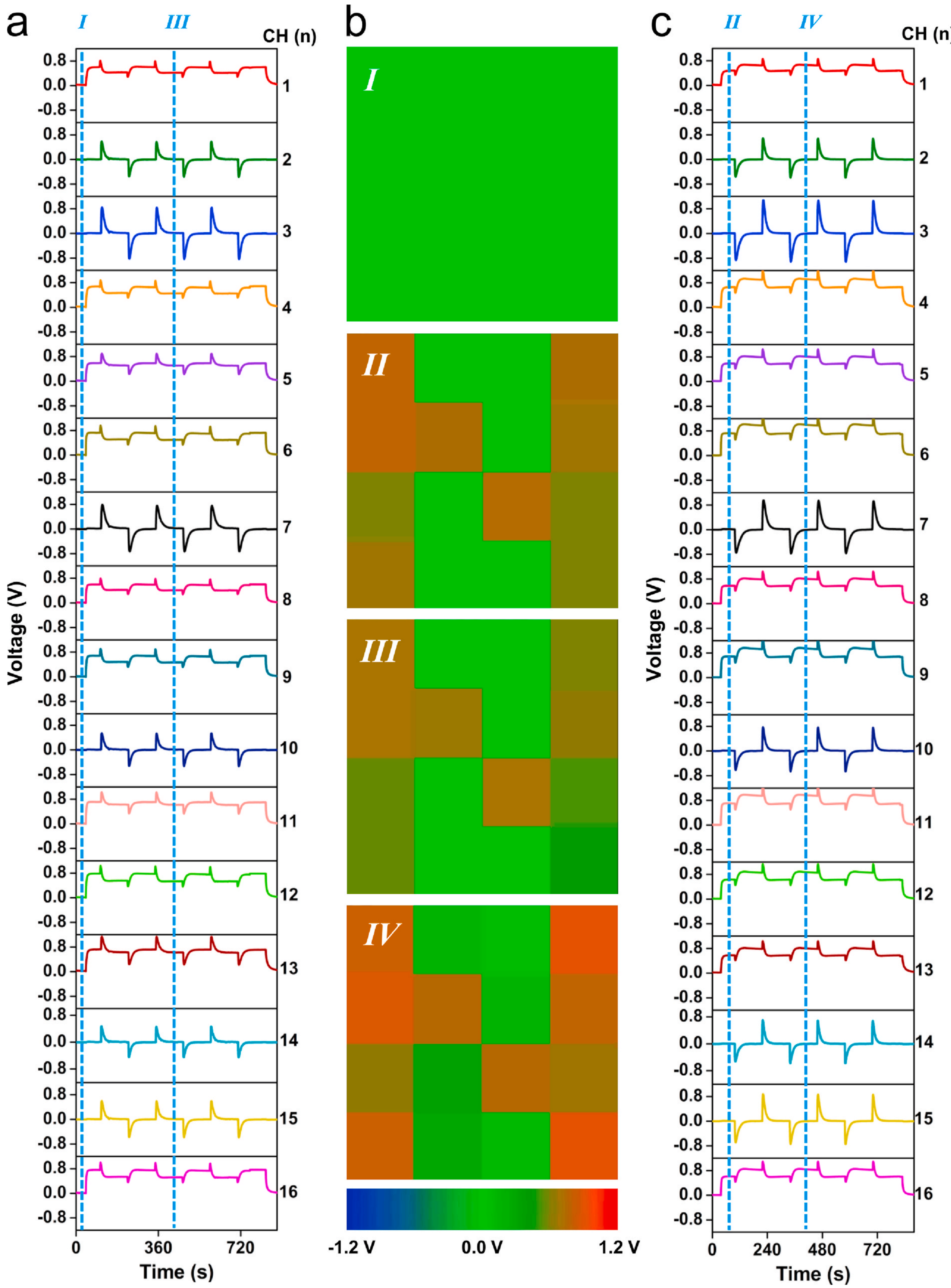


**Fig. 5.** *V-t* curves and mapping images of the self-powered photodetector system under different conditions. (**a**) *V-t* curves of the fabricated self-powered flexible photodetector system under 405 nm illumination (127.6 mW/cm$^2$) through a letter of "N" with a heating condition ($\triangle T = 22.1$ K). (**b**) Voltage Mappings of the self-powered photodetector system under "without light " (*I*), "light " (*II*), "light + heating" (*III*) and "light + cooling" conditions (*IV*). (**c**) *V-t* curves of the fabricated self-powered flexible photodetector system under 405 nm illumination (127.6 mW/cm$^2$) through a letter of "N" with a cooling condition ($\triangle T = -14.5$ K).

order to improve the output performance of the device, a higher polarization voltage was selected during the polarization process of the ITO/BTO/Ag device.

To demonstrate the possible application of the device, we fabricated a flexible photodetector system using a 4 × 4 photovoltaic-pyroelectric sensing matrix array of 16 ITO/BTO/Ag units and a kapton film. The 4 × 4 ITO/BTO/Ag array was attached to a kapton film and integrated to form a flexible device, as illustrated in Fig. 4a–c and Fig. S15 (Supporting Information). The flexible photodetector system was able to bend at a range of curvatures to adapt to the changing testing position, as shown in Fig. 4b and c. More importantly, the 16 BTO sensor units were connected to a multichannel data acquisition system to gather sensing data. The voltage-time (*V-t*) curves of 16 channels induced via the illumination (127.6 mW/cm$^2$) are illustrated in Fig. 4d and Fig. S16. The recorded voltage plateau range was 0.58 V–0.77 V, indicating that each unit of the photodetector system exhibits good stability and presented a similar voltage signal when the light was on/off. The data in Fig. S16 (Supporting Information) is displayed to quantify the low variability of the individual measurements. Moreover, Fig. 4e and Fig. S17 (Supporting Information) display the *V-t* curves when illumination was used for the self-powered systems through a mask with a "N" (Fig. 4e), "U" and "O" shape on it. The corresponding mapping images are presented in Fig. S18 (Supporting Information). Showing that the channels that receive light have typical output voltage signals, while the light blocked channels do not detect signals. In addition, each unit of the photodetector systems shows good pyroelectric properties, see Fig. S19 (Supporting Information), and photovoltaic-pyroelectric coupled properties, Fig. S20 (Supporting Information), where the measured voltage of every ITO/BTO/Ag unit increases with increasing illumination intensity from 31.7 mW/cm$^2$ to 127.6 mW/cm$^2$ (mask with "N") and the output voltage presents a better linear relationship with the illumination intensity. Meanwhile, the measured output voltage signal of each ITO/BTO/Ag unit of the self-powered system is quite independent, sensitivity and no interference were seen from neighboring units, which shows that the dependability of the flexible photodetector systems (Fig. S21, Supporting Information).

Fig. 5 presents the voltages and the mapping images of photodetector system using a mask with "N" shape on it under "no light", "light", "light + heating" and "light + cooling" conditions. As displayed in Fig. 5a and c, the channels with an open area record photovoltaic-pyroelectric coupled signals, but the sheltered channels with no light only exhibit a pyroelectric response. According to the four conditions, the voltage-curves and mapping images (Fig. 5b) of the self-powered flexible photodetector systems can be divided into four stages as follows: In the phase *I*, the voltage mapping of the system show the same green color without light applied, consistent with the blue line labeled "*I*" in Fig. 5a where the voltages were not obtained. In the phase *II*, on illuminating the device with light, an obvious color change can be seen on the non-masked areas, while the masked areas maintained the same green color. Under "light + heating" state, the lowest voltage plateau is obtained in the non-masked channels (phase *III*). The highest voltage plateau is recorded in non-masked channels of the photodetector system experiencing "light + cooling" (phase *IV*). The result indicates the voltage plateau of system under "light" (*II*), "light + heating" (*III*) and "light + cooling" (*IV*) states. Moreover, the designed self-powered flexible photodetector system has good stability and repeatability under different conditions, as presented in Figs. S22–S25 (Supporting Information). The overlay data of *V-t* curves of the photodetector system demonstrates the small variability and quantify the variability of the responses of the individual measurements (Fig. S26, Supporting Information).

## 4. Conclusion

In summary, our findings demonstrate a novel photovoltaic-pyroelectric system capable of simultaneous sensing using highly responsive ferroelectric BTO sheets. Under light illumination and cooling simultaneously, the fabricated flexible photodetector system delivers an enhancement of photocurrent and photovoltage plateaus owing to ferro-pyro-phototronic effect. The corresponding photoconductive gain, specific detectivity and responsivity of the photodetector can be boosted by over 160% at an illumination intensity of 127.6 mW/cm$^2$ as compared with that of using the photovoltaic effect alone. The 4 × 4 photovoltaic-pyroelectric sensing matrix array of BTO has been demonstrated to achieve a flexible photodetector system for detection of ambient light illumination and temperature variations by real-time reflecting the voltages of 16 ITO/BTO/Ag units as a 4 × 4 mapping array. The BTO materials with ferro-pyro-phototronic effect provides potential for future technologies and applications such as wearable electronics, environmental sensors and artificial intelligent sensors.

## Credit author contribution statement

**Kun Zhao:** All authors contributed to data analysis and commented on the manuscript, fabricated the devices and performed measurements, discussed experimental results, drew figures, and prepared the manuscript. **Bangsen Ouyang:** All authors contributed to data analysis and commented on the manuscript, fabricated the devices and performed measurements, discussed experimental results, drew figures, and prepared the manuscript. **Chris R. Bowen:** All authors contributed to data analysis and commented on the manuscript, discussed experimental results, drew figures, and prepared the manuscript. All authors contributed to data analysis and commented on the manuscript. **Ya Yang:** All authors contributed to data analysis and commented on the manuscript, conceived the idea and guided the project, discussed experimental results, drew figures, and prepared the manuscript.

## Declaration of competing interest

The authors declare that they have no known competing financial interests or personal relationships that could have appeared to influence the work reported in this paper.

## Acknowledgments

This work was supported by the National Key R&D Program of China (Grant No. 2016YFA0202701), the National Natural Science Foundation of China (Grant Nos. 51472055), External Cooperation Program of BIC, Chinese Academy of Sciences (Grant No. 121411KYS820150028), the 2015 Annual Beijing Talents Fund (Grant No. 2015000021223ZK32), Excellent Youth Talent Training Programs of Laboratory of Advanced Processing and Recycling of Nonferrous Metals, Lanzhou University of Technology (No.201904), the 2020 Annual Gansu University Innovation Fund Project (No. 2020A-018), Qingdao National Laboratory for Marine Science and Technology (No. 2017ASKJ01), the University of Chinese Academy of Sciences (Grant No. Y8540XX2D2), and the "thousands talents" program for the pioneer researcher and his innovation team, China.

## Appendix A. Supplementary data

Supplementary data to this article can be found online at https://doi.org/10.1016/j.nanoen.2020.105152.

## References

[1] Z.L. Wang, Mater. Today 20 (2017) 74–82.
[2] C. Zhang, W. Tang, Y. Pang, C. Han, Z.L. Wang, Adv. Mater. 27 (2015) 719–726.
[3] F.R. Fan, W. Tang, Z.L. Wang, Adv. Mater. 28 (2016) 4283–4305.
[4] J. Feng, M. Graf, K. Liu, D. Ovchinnikov, D. Dumcenco, M. Heiranian, V. Nandigana, N.R. Aluru, A. Kis, A. Radenovic, Nature 536 (2016) 197–200.
[5] J.-H. Lee, H.-J. Yoon, T.Y. Kim, M.K. Gupta, J.H. Lee, W. Seung, H. Ryu, S.-W. Kim, Adv. Funct. Mater. 25 (2015) 3203–3209.

[6] Z. Wang, R. Yu, C. Pan, Z. Li, J. Yang, F. Yi, Z.L. Wang, Nat. Commun. 6 (2015) 8401.
[7] T. Ji, Q. Liu, R. Zou, Y. Sun, K. Xu, L. Sang, M. Liao, Y. Koide, L. Yu, J. Hu, Adv. Funct. Mater. 26 (2016) 1400–1410.
[8] K. Thirumal, H. Ding, C. Yan, W.L. Leong, T. Baikie, L. Zhang, M. Sherburne, S. Li, M. Asta, N. Mathews, S. Gautam Mhaisalkar, J. Mater. Chem. 3 (2015) 23829–23832.
[9] Z. Xiao, Y. Yuan, Y. Shao, Q. Wang, Q. Dong, C. Bi, P. Sharma, A. Gruverman, J. Huang, Nat. Mater. 14 (2015) 193–198.
[10] A. Esin, I. Baturin, T. Nikitin, S. Vasilev, F. Salehli, V.Y. Shur, A.L. Kholkin, Appl. Phys. Lett. 109 (2016) 142902.
[11] N. Ma, Y. Yang, Nano Energy 40 (2017) 352–359.
[12] X. Wang, Y. Dai, R. Liu, X. He, S. Li, Z.L. Wang, ACS Nano 11 (2017) 8339–8345.
[13] F. Zhang, Y. Zang, D. Huang, C. Di, D. Zhu, Nat. Commun. 6 (2015) 8356.
[14] D. Champier, Energy Convers. Manag. 140 (2017) 167–181.
[15] J.-H. Bahk, H. Fang, K. Yazawa, A. Shakouri, J. Mater. Chem. C 3 (2015) 10362–10374.
[16] H. Zhu, Y. Wang, J. Xiao, M. Liu, S. Xiong, Z.J. Wong, Z. Ye, Y. Ye, X. Yin, X. Zhang, Nat. Nanotechnol. 10 (2015) 151–155.
[17] F. Li, D. Lin, Z. Chen, Z. Cheng, J. Wang, C. Li, Z. Xu, Q. Huang, X. Liao, L.-Q. Chen, T.R. Shrout, S. Zhang, Nat. Mater. 17 (2018) 349–354.
[18] G. da C. Rodrigues, P. Zelenovskiy, K. Romanyuk, S. Luchkin, Y. Kopelevich, A. Kholkin, Nat. Commun. 6 (2015) 7572.
[19] L. You, F. Zheng, L. Fang, Y. Zhou, L. Z Tan, Z. Zhang, G. Ma, D. Schmidt, A. Rusydi, L. Wang, L. Chang, A. M Rappe, J. Wang, J. Sci. Adv. 4 (2018) eaat3438.
[20] T. Rojac, A. Bencan, G. Drazic, N. Sakamoto, H. Ursic, B. Jancar, G. Tavcar, M. Makarovic, J. Walker, B. Malic, D. Damjanovic, Nat. Mater. 16 (2017) 322–327.
[21] T. Choi, S. Lee, Y.J. Choi, V. Kiryukhin, S.-W. Cheong, Science 324 (2009) 63–66.
[22] Y. Yang, S. Wang, Y. Zhang, Z.L. Wang, Nano Lett. 12 (2012) 6408–6413.
[23] X. Yang, X. Su, M. Shen, F. Zheng, Y. Xin, L. Zhang, M. Hua, Y. Chen, V.G. Harris, Adv. Mater. 24 (2012) 1202–1208.
[24] K. Zhao, B. Ouyang, Y. Yang, iScience 3 (2018) 208–216.
[25] L. Wu, A.R. Akbashev, A.A. Podpirka, J.E. Spanier, P.K. Davies, J. Am. Ceram. Soc. 102 (2019) 4188–4199.
[26] N. Ma, Y. Yang, Nano Energy 50 (2018) 417–424.
[27] A.M. Glass, D. von der Linde, T.J. NegranK, Appl. Phys. Lett. 25 (1974) 233–235.
[28] L. Arizmendi, Phys. Status Solidi 201 (2004) 253–283.
[29] J. Carnicero, O. Caballero, M. Carrascosa, J.M. Cabrera, Appl. Phys. B 79 (2004) 351–358.
[30] N. Ma, K. Zhang, Y. Yang, Adv. Mater. 29 (2017) 1703694.
[31] K. Song, R. Zhao, Z.L. Wang, Y. Yang, Adv. Mater. 31 (2019) 1902831.
[32] Y. Yang, J.H. Jung, B.K. Yun, F. Zhang, K.C. Pradel, W. Guo, Z.L. Wang, Adv. Mater. 24 (2012) 5357.
[33] S.B. Lang, S.A.M. Tofail, A.A. Gandhi, M. Gregor, C. Wolf-Brandstetter, J. Kost, S. Bauer, M. Krause, Appl. Phys. Lett. 98 (2011) 123703.
[34] D. Zheng, H. Fang, P. Wang, W. Luo, F. Gong, J.C. Ho, X. Chen, W. Lu, L. Liao, J. Wang, W. Hu, Adv. Funct. Mater. 26 (2016) 7690–7696.
[35] L. Zheng, F. Teng, Z. Zhang, B. Zhao, X. Fang, J. Mater. Chem. C 4 (2016) 10032–10039.
[36] L. Zheng, P. Yu, K. Hu, F. Teng, H. Chen, X. Fang, ACS Appl. Mater. Interfaces 8 (2016) 33924–33932.
[37] G. Sanchez-Santolino, J. Tornos1, D. Hernandez-Martin, J.I. Beltran, C. Munuera, M. Cabero, A. Perez-Muñoz, J. Ricote, F. Mompean, M. Garcia-Hernandez, Z. Sefrioui, C. Leon, S.J. Pennycook, M.C. Muñoz, M. Varela, J. Santamaria, Nat. Nanotechnol. 12 (2017) 655–662.
[38] N. Ma, Y. Yang, Nano Energy 60 (2019) 95–102.
[39] Z. Xi, J. Ruan, C. Li, C. Zheng, Z. Wen, J. Dai, A. Li, D. Wu, Nat. Commun. 8 (2017) 15217.
[40] X. Wang, P. Wang, J. Wang, W. Hu, X. Zhou, N. Guo, H. Huang, S. Sun, H. Shen, T. Lin, M. Tang, L. Liao, A. Jiang, J. Sun, X. Meng, X. Chen, W. Lu, J. Chu, Adv. Mater. 27 (2015) 6575–6581.
[41] L. Tu, R. Cao, X. Wang, Y. Chen, S. Wu, F. Wang, Z. Wang, H. Shen, T. Lin, P. Zhou, X. Meng, W. Hu, Q. Liu, J. Wang, M. Liu, J. Chu, Nat. Commun. 11 (2020) 101.
[42] X. Wang, H. Shen, Y. Chen, G. Wu, P. Wang, H. Xia, T. Lin, P. Zhou, W. Hu, X. Meng, J. Chu, J. Wang, Adv. Sci. 6 (2019) 1901050.

**Kun Zhao** received his Ph.D. degree in Material Physics and Chemistry from Beijing Institute of Nanoenergy and Nanosystems, Chinese Academy of Sciences (CAS) in 2018. He is currently an associate professor at State Key Laboratory of Advanced Processing and Recycling of Nonferrous Metals, Lanzhou University of Technology. His main research interests focused on energy harvesting and fabrication of nano-devices, triboelectric nanogenerator, self-powered wireless sensors and new energy technology.

**Bangsen Ouyang** is a Ph.D student in the research group of Professor Ya Yang at Beijing Institute of Nanoenergy and Nanosystems, Chinese Academy of Sciences (CAS). He received his bachelor's degree in Applied Physics from Xihua University in 2014. His current interests focus on self-powered photodetector.

**Prof. Chris R. Bowen** has a BSc degree in Materials Science from the University of Bath (1986–1990) and a DPhil from the University of Oxford (1990–1993). Post-doctoral work was at Tecnische Universität Harburg-Hamburg and University of Leeds (1994–1996). He was Senior Scientist at the Defence Evaluation and Research Agency from 1996 to 1998. He joined Bath as a Lecturer in 1998 and is now Professor of Materials. Research includes energy harvesting, ferroelectrics and functional ceramics.

**Prof. Ya Yang** received his Ph.D. in Materials Science and Engineering from University of Science and Technology Beijing, China. He is currently a professor at Beijing Institute of Nanoenergy and Nanosystems, Chinese Academy of Sciences, China. He has developed various new hybridized and multi-effects coupled nanogenerators, opening up the new principles of the device design and coupled effects, and the new approaches of improving output performances of energy-related devices. His main research interests focus on the field of hybridized and coupled nanogenerators for energy conversion, self-powered sensing, and some new physical effects. Details can be found at: http://www.researcherid.com/rid/A-7219-2016.